An experimental study on the early diagnosis of traumatic brain injury in rabbits based on a noncontact and portable system

Jun Yang[1,*], Hui Zhao[2,*], Gen Li[3], Qisheng Ran[4], Jingbo Chen[1], Zelin Bai[1], Gui Jin[1], Jian Sun[1], Jia Xu[1], Mingxin Qin[1] and Mingsheng Chen[1]

[1] College of Biomedical Engineering, Army Medical University, Chongqing, China
[2] State Key Laboratory of Trauma, Burns and Combined Injury, Institute of Surgery Research, Third Military Medical University, Chongqing, China
[3] Department of Biomedical Engineering, Chongqing University of Technology, Chongqing, China
[4] Department of Radiology, Army Medical Center, Chongqing, China
* These authors contributed equally to this work.

Corresponding authors
Mingxin Qin,
qmingxin@tmmu.edu.cn
Mingsheng Chen,
chenms83@tmmu.edu.cn

ABSTRACT

Closed cerebral hemorrhage (CCH) is a common symptom in traumatic brain injury (TBI) patients who suffer intracranial hemorrhage with the dura mater remaining intact. The diagnosis of CCH patients prior to hospitalization and in the early stage of the disease can help patients get earlier treatments that improve outcomes. In this study, a noncontact, portable system for early TBI-induced CCH detection was constructed that measures the magnetic induction phase shift (MIPS), which is associated with the mean brain conductivity caused by the ratio between the liquid (blood/CSF and the intracranial tissues) change. To evaluate the performance of this system, a rabbit CCH model with two severity levels was established based on the horizontal biological impactor BIM-II, whose feasibility was verified by computed tomography images of three sections and three serial slices. There were two groups involved in the experiments (group 1 with 10 TBI rabbits were simulated by hammer hit with air pressure of 600 kPa by BIM-II and group 2 with 10 TBI rabbits were simulated with 650 kPa). The MIPS values of the two groups were obtained within 30 min before and after injury. In group 1, the MIPS values showed a constant downward trend with a minimum value of $-11.17 \pm 2.91°$ at the 30th min after 600 kPa impact by BIM-II. After the 650 kPa impact, the MIPS values in group 2 showed a constant downward trend until the 25th min, with a minimum value of $-16.81 \pm 2.10°$. Unlike group 1, the MIPS values showed an upward trend after that point. Before the injury, the MIPS values in both group 1 and group 2 did not obviously change within the 30 min measurement. Using a support vector machine at the same time point after injury, the classification accuracy of the two types of severity was shown to be beyond 90%. Combined with CCH pathological mechanisms, this system can not only achieve the detection of early functional changes in CCH but can also distinguish different severities of CCH.

INTRODUCTION

Traumatic brain injury (TBI) is a term indicating brain function changes or brain pathological changes caused by external forces acting on the head, which results in both high morbidity and mortality, particularly for people under 45 years of age (*Zeiler et al., 2017*; *Namjoshi et al., 2013*). A TBI occurs every 15 s, generating 1.7 million new brain injury victims per year in the US. These cases are annually responsible for 50,000 deaths and lead to 80,000 individuals with permanent disabilities (*Prins et al., 2013*). Motor vehicle accidents, falls and explosive blasts are the major causes of closed cerebral hemorrhage (CCH) (*Wang et al., 2006*; *Pugh et al., 2016*; *Namjoshi et al., 2013*).

As time progresses, CCH can be divided into two stages. One is the acute hemorrhage stage, with a rapid accumulation of blood, and the other is the chronic hemorrhage stage, with a gradual increase in intracranial pressure (ICP). Due to the dynamics of hematoma expansion, the primary damage occurs within minutes to hours after the injury and is a result of mechanical damage. Secondary injuries gradually occur as a consequence of ongoing cellular events that cause further damage. Many parallel pathological pathways exist, including: (1) Ion channel augmentation; (2) hypermetabolism; (3) excitotoxicity; (4) spreading depression; and (5) oxidative stress and inflammation (*Kaur & Sharma, 2018*; *Davis, 2000*; *Namjoshi et al., 2013*; *Prins et al., 2013*; *Aronowski & Zhao, 2011*; *Chen, 2003*). A delay in treatment will cause poor patient outcomes and death because of the accumulation of blood over time (*Indraswari et al., 2012*). Hence, there is a need for early techniques prior to hospitalization to diagnose occult injuries such as CCH from clinical observations.

The clinical golden standard for detecting CCH is computed tomography (CT), which can rapidly achieve both accuracy and quantitation in diagnosis. The main limitation of CT is that it is not suited for use in all regions, such as in remote villages, because of its bulk mass and operational complexity (*Pandey et al., 2017*; *Amrhein et al., 2017*). Although mobile CT units are developing, they are too rigorous for vehicles and rarely used roads, and their sensitivity and specificity are lower than those of a CT in a radiological chamber (*Schwindling et al., 2016*). Another common method of clinical management for CCH patients is ICP monitoring, which allows the real-time and accurate monitoring of ICP changes by implanting a microelectrode probe into the skull. There are high risks, however, for a secondary hemorrhage and infection (*Giraudet et al., 2017*; *Liljacyron et al., 2018*). Although CT imaging can achieve noncontact detection, it cannot perform real-time monitoring bedside due to its bulky size and low temporal resolution. ICP monitoring is the inverse of CT. Neither method can simultaneously achieve the requirements of noncontact and real-time monitoring to detect CCH. Currently, there is lack of safe and real-time diagnostic methods for CCH, or even TBI. In recent decades, many groups have reported detection methods used for the diagnosis of TBI, such as near-infrared spectroscopy (NIRS) and electrical impedance tomography (EIT).

The detection principle of NIRS is to compare the near-infrared light absorption of the left and right brain hemispheres. The light value absorbed by the instrument is asymmetric on the two sides of the skull for TBI patients, which can demonstrate a hematoma on the side with the largest absorption. A detection sensitivity of 88% and a specificity of 90.7% for intracranial hemorrhage were shown by *Robertson et al. (2010)*. However, the result is only for a hemorrhage larger than 3.5 ml, within 2.5 cm from the scalp. With no hemorrhage size limiting, the sensitivity decreases to 68.7% (*Robertson et al., 2010*). The NIRS has no advantage in the detection of the deep brain and small details. EIT is a functional imaging technique that images the electrical property distribution of the brain by safely injecting electrical currents into the surface of the skull and measuring the boundary voltages through specific electrodes. However, a shortcoming of EIT is that the cranium has a high electrical insulation that limits current penetration and restricts deep imaging of the brain without using invasive implanted electrodes (*Koessler et al., 2017*; *Song et al., 2018*; *Manwaring et al., 2013*).

Exploring the brain injury in a safe, noninvasive manner has become popular in recent decades. Microwave or radar technology can describe the development of TBI by monitoring the change of impendance characteristic (*Mobashsher, Abbosh & Wang, 2014*; *Oziel, Korenstein & Rubinsky, 2017*). Literally, monitoring the phase shift and the resonance frequency can attain more comprehensive information of dielectric properties which reflect the change of cranial contents (*Gonzalez et al., 2013*; *Gonzalez & Rubinsky, 2006*; *Griffith et al., 2018*; *Kellner et al., 2018*). In this study, a method based on the magnetic induction phase shift (MIPS) is proposed to detect high incidence of CCH in TBI for an early diagnosis. The MIPS technique is a safe, noncontact, real-time and new method for the detection of brain lesions that utilizes the changes in the dielectric properties of biological tissues to extract pathophysiology information of tissues. Since different types of tissues and organs exhibit different electrical properties, this method uses a single frequency signal that generates an alternating main magnetic field to pass through biological tissues that measures changes of tissue conductivity caused by the disturbing magnetic field (*Jin et al., 2014a*; *Jin et al., 2014b*). In our previous work, *Jin et al. (2014b)*. designed a MIPS detection system based on a Tektronix signal source and a PXI platform to study intracranial hemorrhage in rabbits with a contralateral hemisphere cancellation coil by injection of a self-body blood model and discovered that the MIPS technique enables noncontact diagnosis and is sensitive to intracranial hemorrhage. But the model established by an intracranial injection of external blood differs from that of clinical TBI conditions. *Li et al. (2017a)* and *Sun et al. (2016)* showed that the MIPS technique is more sensitive than ICP monitoring when detecting brain lesions, demonstrating that the MIPS technique can achieve early detection in real-time. However, for TBI-induced CCH the ICP cannot increase immediately because of the effect of cerebral autoregulation (*Cernak, 2006*; *Di Ieva, Schmitz & Cusimano, 2013*). Therefore, this study aimed to investigate whether the MIPS method can perform an early diagnosis of TBI-induced CCH.

To obtain more information in the wide band in this study, we designed a magnetic induction brain monitor capable of measuring MIPS values from 300 kHz to 300 MHz. In addition, we established a cortical impact rabbit model based on the horizontal

Magnetic Induction Brain Monitor
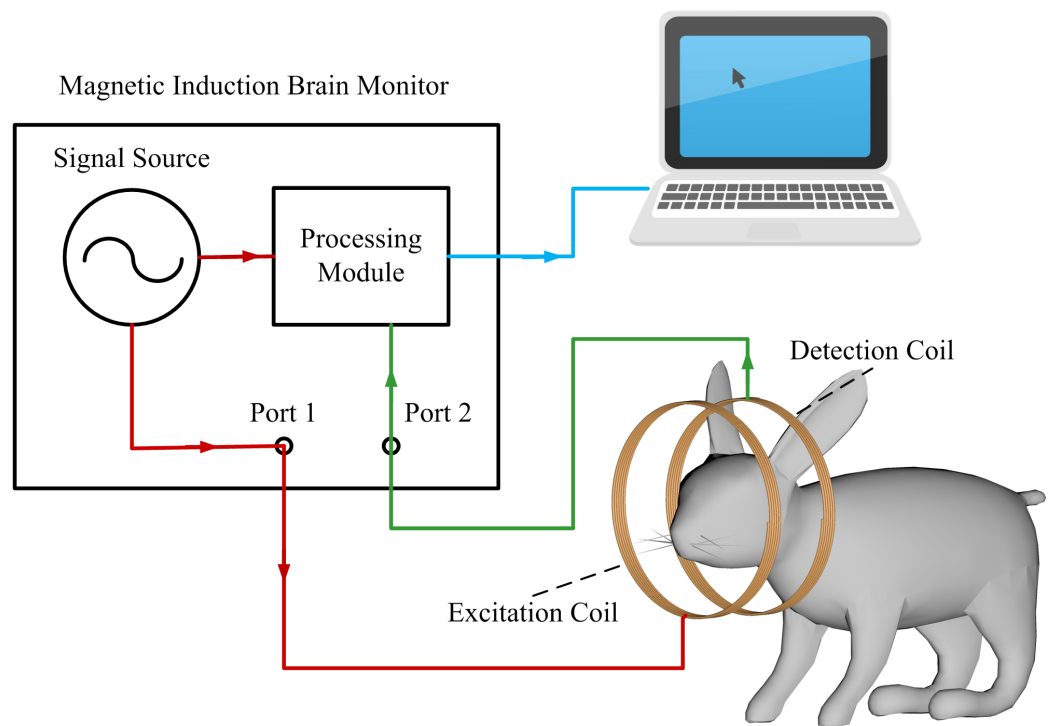
Figure 1 The schematic of the detection system.

biological impactor BIM-II. Subsequently, with the self-designed monitor and coil sensor, we collected the MIPS data, which can reflect the change of mean brain conductivity caused by two CCH severity levels within 30 min of an injury. Additionally, the feasibility of this model was verified via CT images of three sections and serial slices 1 h after injury. Finally, the accuracy of CCH severity classification was determined based on a support vector machine (SVM) used to evaluate the performance of the MIPS method. We hope that the MIPS technique may serve as a new potential diagnostic method for prehospital diagnosis of CCH after a TBI, which can offer an early diagnosis program for CCH patients and carry out earlier treatments.

MATERIALS AND METHODS

Detection system

The detection system of CCH primarily included a magnetic induction brain monitor (CNJY-2015; Tianda Instrument Company, Chengdu, China) and a coil sensor connected to two high frequency coaxial transmission lines. To better observe signal changes, we connected an external display screen, as shown in Fig. 1.

Magnetic induction brain monitor is an instrument with two ports whose excitation signal from source with a frequency range of 300 kHz–3 GHz and the direct digital frequency synthesis. The source formed two identical signals with the same amplitude, frequency range and initial phase via separation module, one of which received from Port 1 to Port 2 by the processing module, and another as reference signal output to it alike. Then, the processing module performed differential operations on above the two signals.
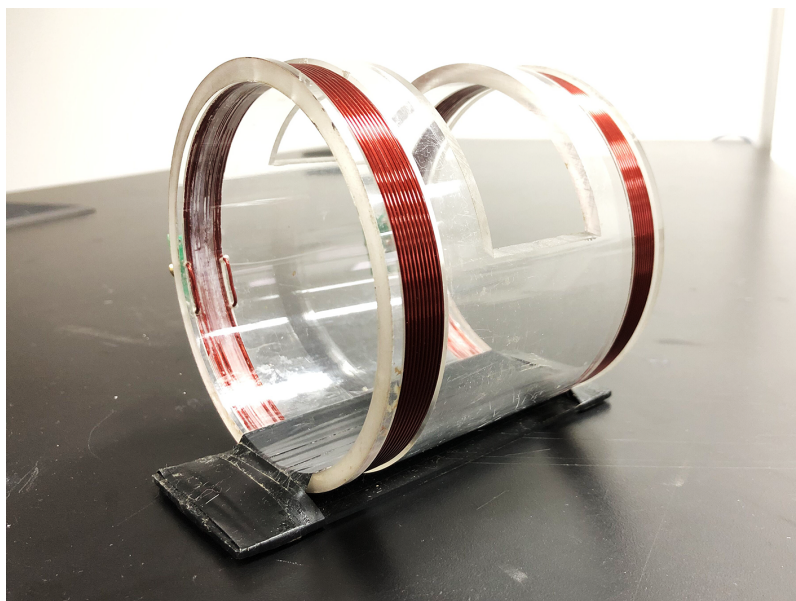
Figure 2 The two-coil sensor. Photograph by Jun Yang.

The coil sensor included the excitation coil and detection coil, as shown in Fig. 2. Both coils are wound with a one mm diameter AWG32 copper enameled wire at two terminals of the plexiglass tube with 10 winding turns. According to the size of a rabbit's skull, we designed the radius of the two coils to be 5.2 cm and the distance between the coils to be 10 cm, to fit the rabbits' heads into the coil.

Detection principle

The excitation signal output from Port 1 generates a main magnetic field through the excitation coil through the output of Port 1. The main magnetic field can penetrate the target to generate an induced eddy current inside, thereby forming a disturbing magnetic field. The detection coil receives the vector addition of the main field and the disturbing magnetic field, named the superimposed magnetic field, which is transmitted to Port 2. The excitation signal partly transmitted from Port 1 to Port 2 via the target was defined as the transmission coefficient, and the remaining signal that did not pass through the target but was reflected to Port 1 was defined as the reflection coefficient that contained less information about the changes to the internal dielectric coefficient of the target than that of the transmission coefficient. Therefore, the data we used was taken from the transmission coefficient. Due to the directional coupler, the reflected signal and the transmitted signal do not interfere with each other.

$$\text{Reflection coefficient} = \frac{V_{\text{reflection}}}{V_{\text{excitation}}} = r \angle \phi$$

$$\text{Transmission coefficient} = \frac{V_{\text{transmission}}}{V_{\text{excitation}}} = t \angle \psi$$

where r and t are the amplitude of reflection coefficient and transmission coefficient, respectively. ϕ and ψ are the phase of reflection coefficient and transmission coefficient, respectively.

According to two-port network testing principle, the change in the impedance properties of the target will affect its conductivity, which is consistent with the MIPS theory (*Griffiths, Stewart & Gough, 1999*; *Sun et al., 2014*). In this study, the target is the brain, and there is a phase in the transmission coefficient called θ between the main magnetic field and the superimposed magnetic field (*Nitsch, Rambousky & Tkachenko, 2015*),

$$\theta = \text{arctg}(P\mu_0\omega\sigma)$$

and the changes in mean brain conductivity that are caused by an alteration in the proportion of intracranial tissue volume are a result of the shifts in phase ($\Delta\theta$) of the current flow through the coil between t_1 and t_2.

$$\Delta\theta = \text{arctg}(P\mu_0\omega\Delta\sigma) = \theta_{t_2} - \theta_{t_1}$$

where P and μ_0 are the target geometry and permeability of free space, both of which have a constant value, ω and σ are the angular frequency and conductivity, respectively, which both have variable values. Hence, $\Delta\theta$ is related to the frequency $f\left(\frac{\omega}{2\pi}\right)$ and the change in conductivity $\Delta\sigma$, when the circuit structure is stable.

Here, $\Delta\theta$ is the MIPS value that we use to reflect changes of the mean brain conductivity caused by CCH between t_1 and t_2.

$$\text{MIPS} = \Delta\theta = \theta_{t_2} - \theta_{t_1}$$

Measurement parameter

The frequency range of the excitation source was set from 300 kHz to 300 MHz. It was enough to set the number of scanning points to 1,001, to reduce the delay in data entry. The output power was adjusted to a maximum of 10 dBm for larger power transmission. The magnetic induction brain monitor can automatically trigger continuous scanning and sample data six times/min for 30 min. The data format that we saved to the system was set to amplitude and phase. After completing the above parameter settings, we performed the detection of rabbit CCH 30 min before and after injury.

No-load measurement of detection system

Detection system maintained stable after short time of warming up under no-load circumstance (temperature drift less than 0.3°). Furthermore, in the frequency range of 300 kHz–300 MHz, we determined the amplitude-frequency characteristics of the reflection coefficient and the transmission coefficient, which was the power amplitude-frequency characteristics of the two ports when the coil sensor remained unloaded, as shown in Fig. 3. It showed that there was maximum power transmission, but lower power reflection, at 67.14 MHz, which illustrated that Port 2 received the maximum power transmission signal and a small reflection, that is, the signal source and the coil sensor formed the best impedance matching at this frequency. As a result, the MIPS value reached the highest sensitivity.
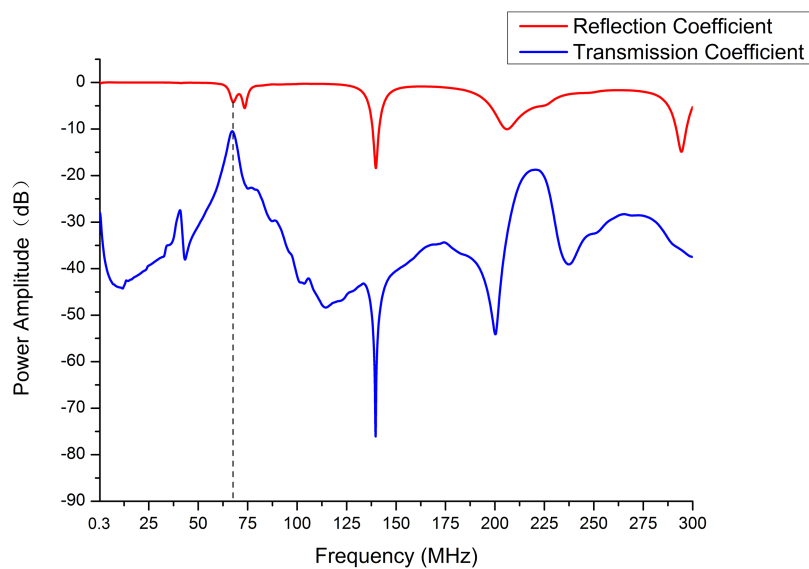
Figure 3 **The power amplitude of reflection and transmission coefficient were measured in the frequency range of 300 kHz to 300 MHz.** Dash line indicates maximum power amplitude of transmission coefficient and relatively lower power amplitude of reflection coefficient at 67.14 MHz.

Experimental design

All animal experiments were carried out in accordance with the guidelines of the Regulations on the Administration of Animal Experiment in Medical Research promulgated by the Ministry of Health of China. The protocol used was approved by the Laboratory Animal Welfare and Ethics Committee of the Third Military Medical University (SYXK-20170002). All efforts were made to minimize the pain of animals in the experiment. A total of 27 New Zealand white rabbits (2.2–2.7 kg, average body weight of 2.4 kg) were selected, and five died in the experiment. The remaining 22 rabbits were randomly divided into three groups (marked Nos. 1–20), composed of a group 1 (Nos. 1–10, $n = 10$), a group 2 (Nos. 11–20, $n = 10$) and a CT control group (Nos. 21–22, $n = 2$).

This experiment lead to rabbit CCH using the horizontal biological impactor BIM-II (Army Medical Center of PLA, Chongqing, China) and the cortical impact method. The impactor consisted of an air gun, a secondary hammer, a pedestal, a universal slab, a high-pressure gas source and a console with a maximum impact speed of 150 km/h. In group 1 and group 2, rabbits started with anesthetization via an ear vein injection of pentobarbital (3%, one ml/kg) and then the hair on the top of the head was removed. The rabbits under anesthesia were placed on the universal slab of the impactor. Then, by adjusting the place of the rabbit's head, the hammer was aimed at the point of the head with one mm in the back of the coronal line and six mm to the right of the sagittal line, as shown in Fig. 4A. Air pressure was set to 600 kPa for group 1 and group 2, respectively. The stroke time were recorded as 37 ms with a high speed camera (Phantom V4.3; Wayne, NJ, USA), respectively.

Figure 4B describes that each rabbit in group 1 and group 2 was placed into the coil sensor before and after the impact injury, positioned by point light locator with caliper tool to maintain consistent. According to the set parameters, the magnetic induction brain

Figure 4 Experimental setup of CCH. Horizontal biological impactor BIM-II (A). CCH detection system in rabbits (B). CT image acquisition of a rabbit (C). Photographs by Jun Yang.

monitor continuously measured the MIPS value in the normal and injured conditions for 30 min with a data sampling rate of once every 10 s, controlled by system software. While measuring, the transient data of the MIPS value can be displayed on the monitor.

CT analysis

Computed tomography imaging was used to get a semiquantitative consequence of the cerebral hemorrhage in rabbits before injury and 1 h after injury, as shown in Fig. 4C. A multislice spiral CT scanner (GE Lightspeed VCT-64 CT; Boston, Massachusetts, USA) was used to axially scan the head of prostrate rabbits, and the scanning parameters were set as follows: 140 kV, 500 mA, FOV 96.0 mm, rotation time 2 s/r, and a slice thickness of 0.625 mm. The sagittal plane and transverse plane of the rabbit head were reconstructed by the obtained CT data in an image postprocessing workstation (AW4.2; GE Medical Systems, Chicago, IL, USA).

Statistical analysis

All the data were expressed as the mean ± standard deviation from 20 independent experiments in group 1 and group 2. At the selected frequency, the differences in the MIPS values from the scans before and after injury were evaluated using a paired t-test to distinguish whether there is a significant difference in the average deviation. Within 30 min, time correlation with the MIPS value was performed by the Pearson correlation
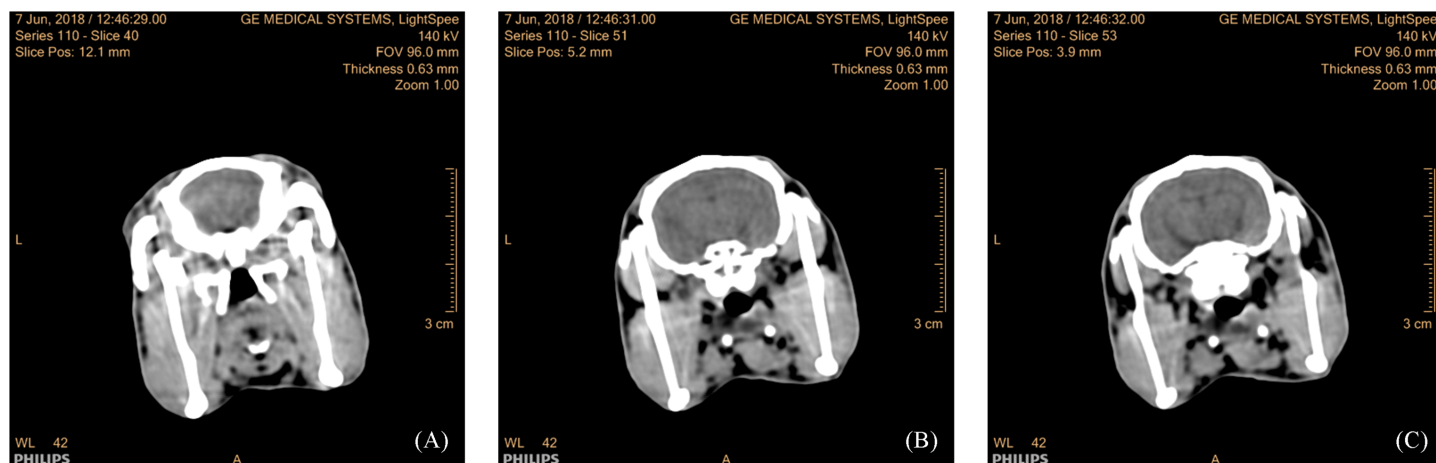
Figure 5 Three-layer coronal CT images of rabbits in the control group. Coronal images of the 40th slice (A), 51st slice (B), 53rd slice (C).

analysis. At the same moment, the significant difference analysis of the MIPS values between group 1 and group 2 was performed using a paired Wilcoxon signed rank test. Statistical analysis was performed using SPSS version 19.0 (SPSS Inc.; Chicago, IL, USA), and p-values under 0.05 were considered significant.

RESULTS

TBI model validation using CT images

Figure 5 presented that there were no clear abnormalities in the brain of the three serial slices in the coronal images of the control group. In group 1 after 1 h of injury via a 600 kPa impact, there were obvious elliptical hemorrhages at the base of the skull in the images from three serial slices and three sections, as shown in Fig. 6. In group 2, after 1 h of injury via a 650 kPa impact, there were obvious strip hemorrhages in the left hemisphere and elliptical hemorrhages in the parietal lobe of serial three-slice and three sections of the images, as shown in Fig. 7. In the coronal position, the number of images with a hemorrhage was five in group 1, and 17 in group 2, revealing that CCH in group 2 had more and wider hemorrhages, based on the morphology and thickness of the hemorrhages. In the CT experiments, the feasibility of the CCH model, which can form a hemorrhage in the impact or hedging location and can lead to two different severity levels, was verified.

MIPS detection result

In the study, five rabbits died after the impact injury, and only two healthy rabbits' CT images were excluded. The remaining 20 rabbits, which maintained a normal heart rate and breathing rate during the measurement period, contributed to the MIPS data. In measurements, the peak value of MIPS at all frequency points ranging from 300 kHz to 300 MHz was selected to be the source data for diagnosis, and the frequency point corresponding to the peak value was called characteristic frequency.
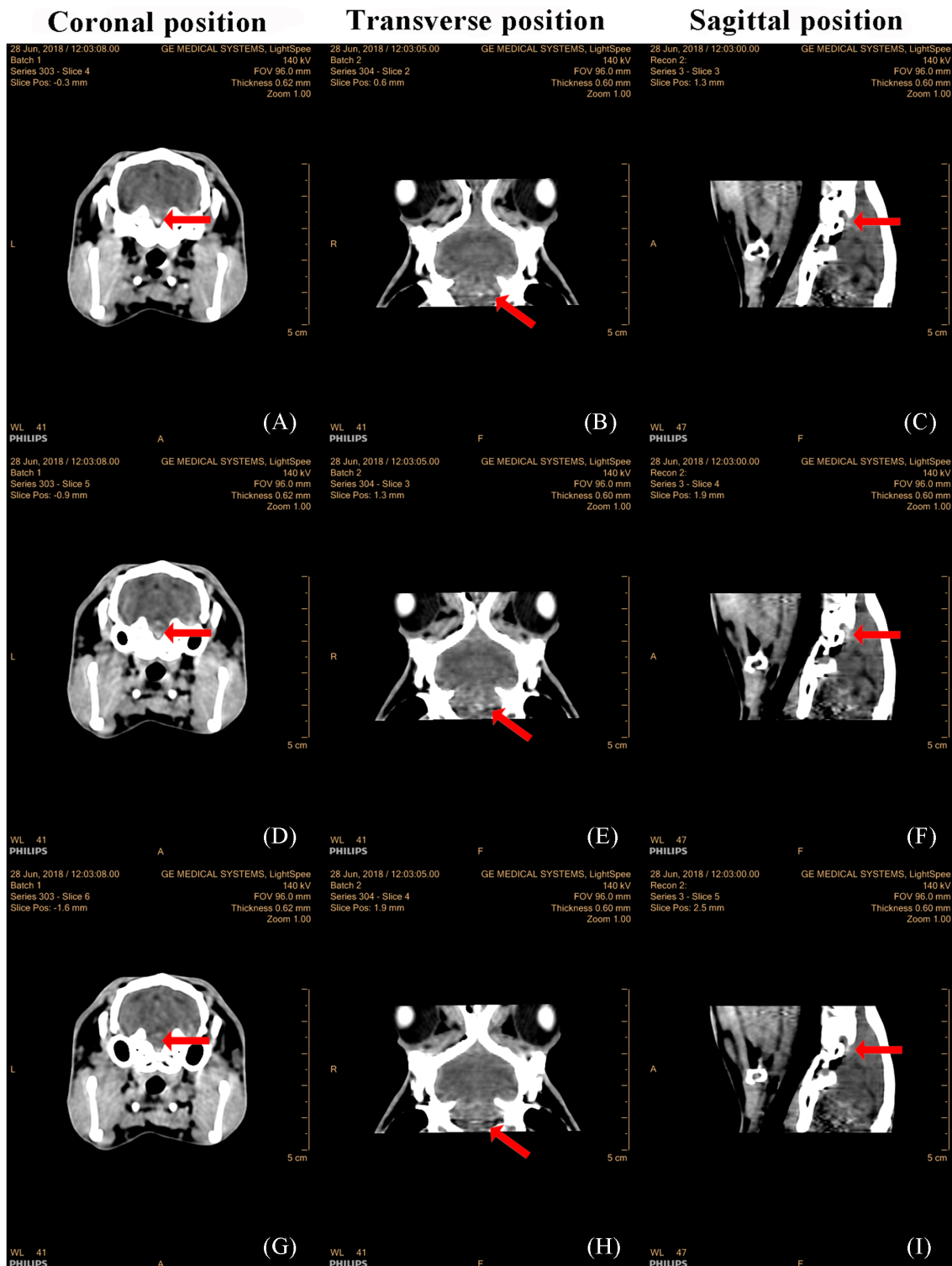
Figure 6 CT images of three serial layers and three sections in group 1, 1 h after injury by a 600 kPa impact. Coronal images of the 4th to 6th slice (A, D, G, respectively). Transverse images of the 2nd to 4th slice (B, E, H, respectively). Sagittal images of the 3rd to 5th slice (C, F, I, respectively).
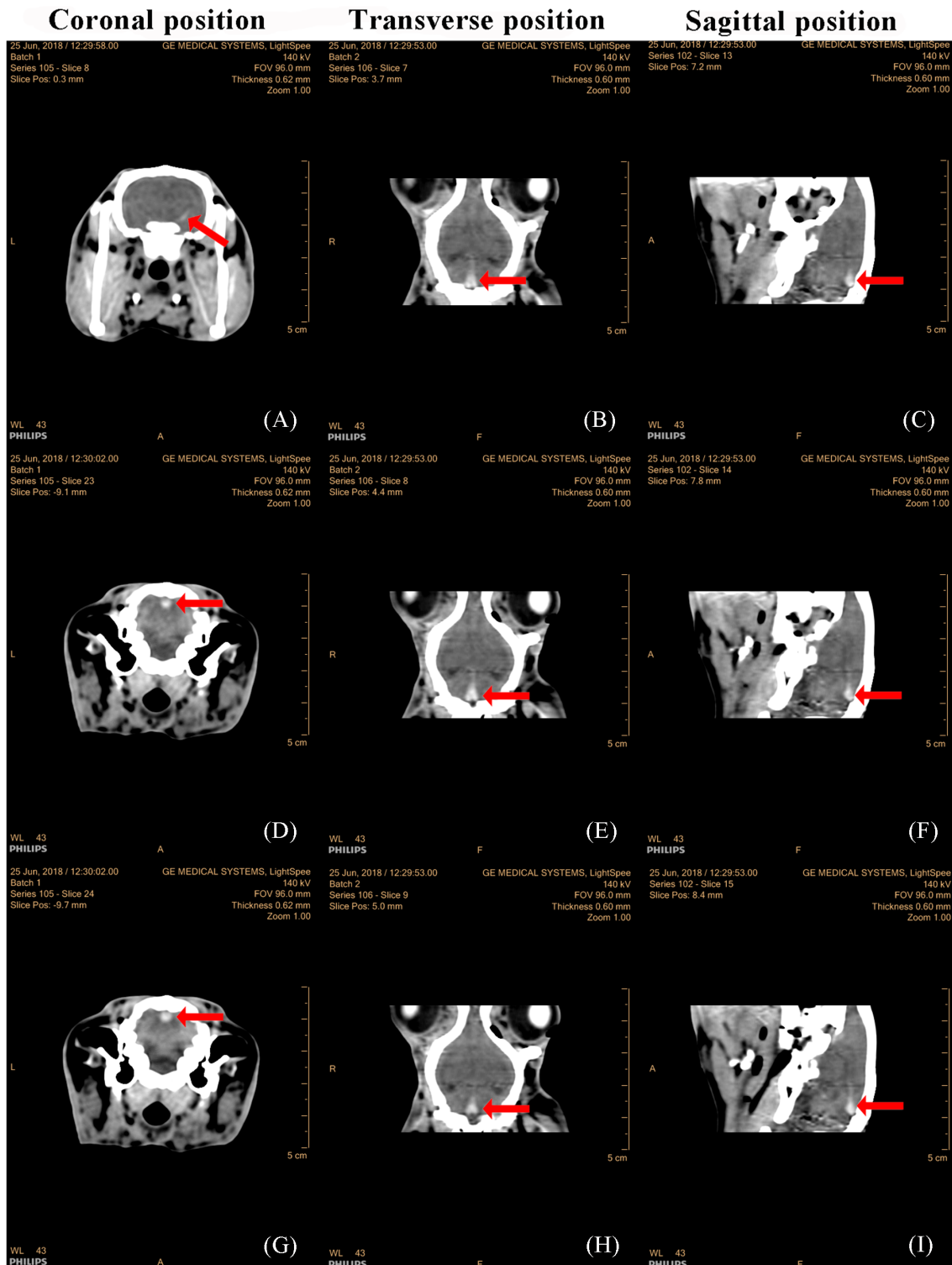
Figure 7 CT images of three serial layers and three sections in group 2, 1 h after injury by a 650 kPa impact. Coronal images of the 8th slice (A), 23th slice (B) and 24th slice (C). Transverse images of the 7th to 9th slice (B, E, H, respectively). Sagittal images of the 13th to 15th slice (C, F, I, respectively).
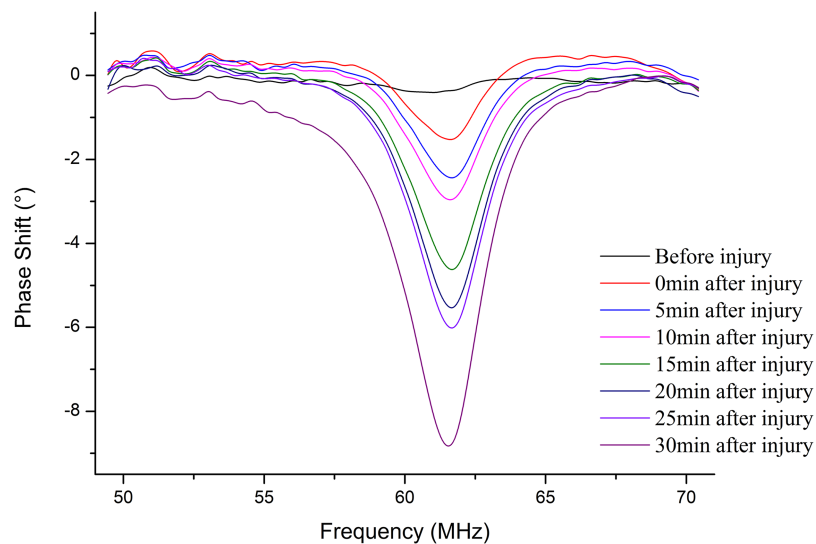
Figure 8 The MIPS curves were plotted before injury and 0 min, 5 min, 10 min, 15 min, 20 min, 25 min, 30 min after injury in the frequency of 50 MHz to 70 MHz.

MIPS in group 1

Figure 8 shows that the MIPS value at characteristic frequency from No. 3 was related to time after injury in the 30 min period. More importantly, the MIPS value stably stayed at approximately 0° before injury, while the MIPS value decreased with time after injury.

Figure 9 shows the mean ± standard deviation trends of MIPS values at 62.61 ± 1.32 MHz within 30 min before injury and 30 min after injury in group 1. The mean MIPS value was −3.77 ± 1.64° at 0 min and −11.17 ± 2.91° after injury and displayed a persistent downward trend. In contrast, there was no clear change to the mean MIPS value, which stayed at approximately 0° before injury (mean MIPS: −0.51 ± 0.58°). A paired t-test analysis with p-value < 0.05 for the same time of the mean MIPS value between before and after injury scans indicated that there was a significant difference between MIPS values before injury and after injury. This result demonstrated that MIPS values can discriminate CCH in group 1. The Pearson correlation coefficient between the mean MIPS value and time was −0.877 before injury (|r| < 0.9). In contrast, the Pearson correlation coefficient was −0.983 after injury (|r| > 0.9). This shows that the trend of the mean MIPS value is not well correlated with time before injury but is closely related to time after injury, which reflects that there was a continuous change in the brain during the measurement. The result indicates that the trend in MIPS values was consistent with the theory that as the pathological process progresses the hemorrhage increased, resulting in a decrease in the mean brain conductivity (*Jin et al., 2014a*; *Laufer, Solomon & Rubinsky, 2012*).

MIPS detection results in group 2

Figure 10 shows that the MIPS value at characteristic frequency from No. 14 was related to time after injury in the 30 min period. Similar to group 1, the MIPS value was

eJ
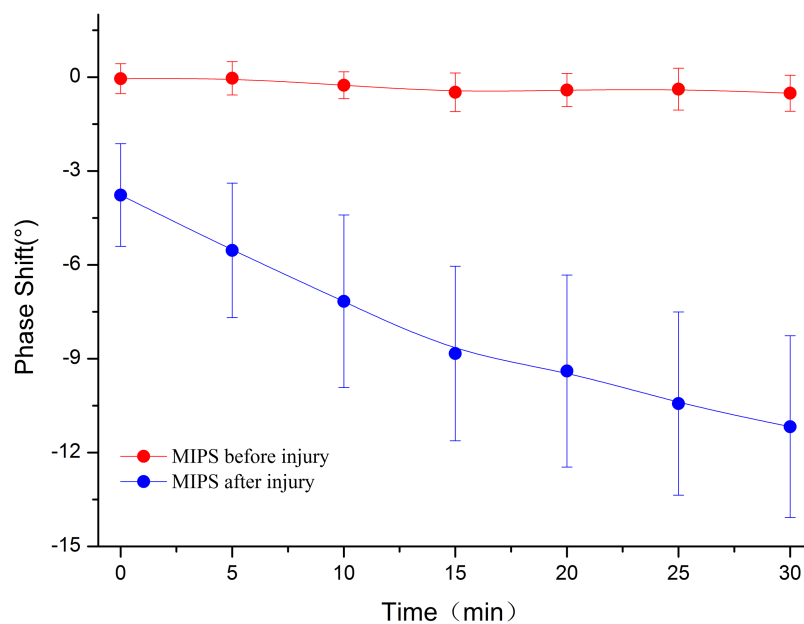
Figure 9 In group 1, the mean ± standard deviation MIPS curve of rabbits were declining within 30 min after injury compared to which before injury.
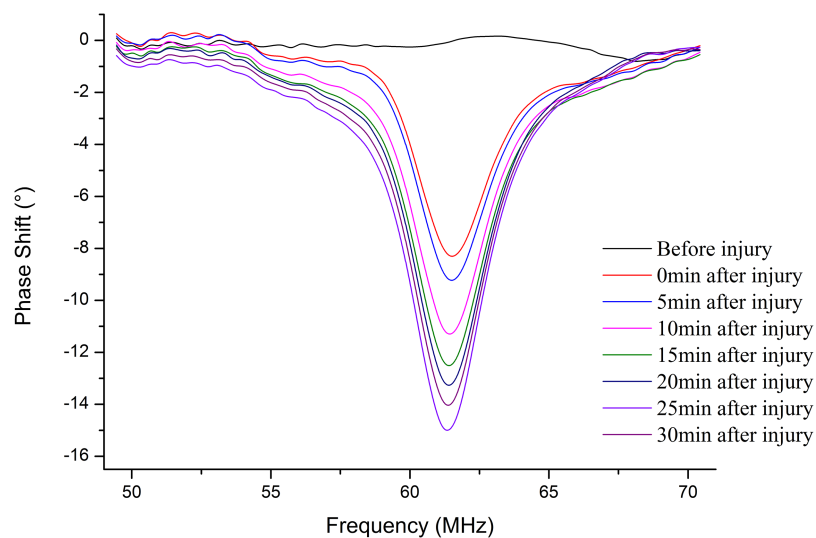
Figure 10 The MIPS curves were plotted before injury and 0 min, 5 min, 10 min, 15 min, 20 min, 25 min, 30 min after injury in the frequency of 50 MHz to 70 MHz.

stable approximately 0° before injury. Unlike group 1, the minimum MIPS value appeared at 25 min, then increased until the end of the measurement. This indicates that the change in mean brain conductivity in No. 14 was not consistent from 0 to 30 min after injury, and there was an inflection point in the later stages of the measurement.

Figure 11 presents the mean ± standard deviation trends of the MIPS values at 62.28 ± 1.10 MHz within 30 min before injury and 30 min after injury in group 2. The mean MIPS value was −9.27 ± 2.34° at 0 min and −16.18 ± 2.22° after injury. In contrast, there
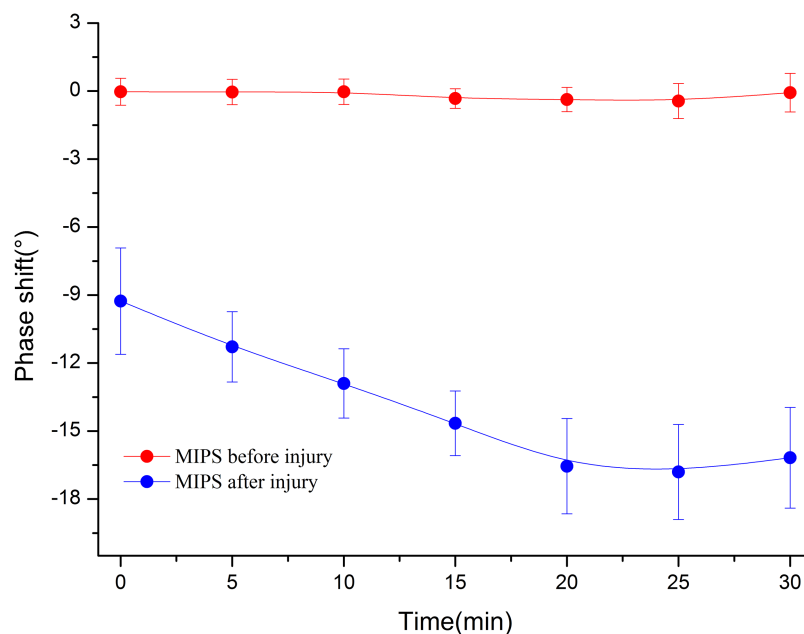
Figure 11 In group 2, the mean ± standard deviation MIPS curve of rabbits declined and then increased slightly after injury, but it remained stable before injury.

was no clear change in the MIPS value, which was stable at approximately 0° before injury (mean MIPS value: $0.44 \pm 0.77°$). Although the trend in the mean MIPS values after injury was similar to that of group 1, it was not completely consistent from 0 to 30 min compared to that of group 1. An inflection point appeared at 25 min (mean MIPS: $-16.81 \pm 2.10°$), then made the mean MIPS values trend upward. A paired t-test analysis with p-value < 0.05 for the same time before and after injury showed that the MIPS value was significantly different before and after injury. This confirms that the MIPS value can discriminate CCH even if the severity increases (e.g., injured by 650 kPa impact). Additionally, a Pearson correlation coefficient between the mean MIPS value and time was -0.527 before injury ($|r| < 0.9$). Conversely, it was -0.942 after injury ($|r| > 0.9$), which reflects CCH expansion over time after injury. Further, the inflection point of the phase curve at 25 min indicates that the mean brain conductivity changes reversed at that time. Hence, the mean brain conductivity decreased before 25 min and then rose after 25 min, which we can infer means that the volume change of certain tissue compositions in the brain reached a critical value, resulting in a reverse change in conductivity at 25 min.

CCH severity classification

In the study, two CCH severity levels besides the normal condition were established by impacting the head of the rabbit with two different pressure values. First, Fig. 12 shows the scatter chart of the MIPS values plotted in 20 rabbits (Nos. 1–20) within 30 min of the injury. Linear fits of the scatter charts were conducted for both group 1 and group 2. The two linearly fitted lines can be considered to be severity level lines. The paired sample Wilcoxon signed rank test for the MIPS values between group 1 and group 2 shows there
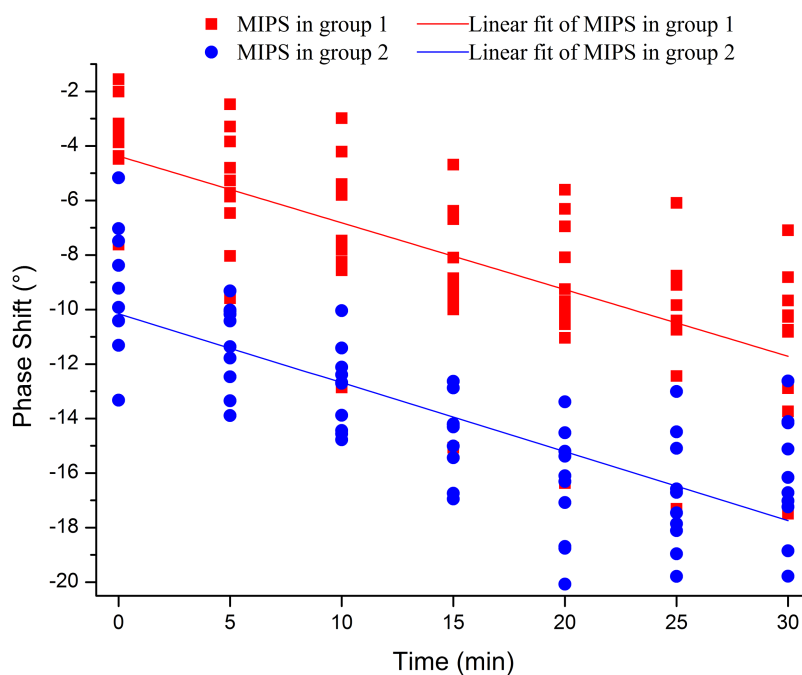
Figure 12 MIPS values of 20 rabbits sampled every 5 min in both two groups within 30 min after injury were plotted as scatter chart. Two linear fits of group 1 and group 2 were calculated by these scatters.

Tables 1 MIPS classification accuracy of two CCH severity levels in rabbits.

Time (min)	0	5	10	15	20	25	30
MIPS accuracy	90%	90%	90%	100%	90%	90%	90%

was a significant difference in the data for group 1 and group 2 (*p*-value < 0.05). The linear fits of scatter and statistical analysis intuitively and qualitatively confirm that the MIPS value can distinguish the severity of rabbit CCH.

To test the accuracy of CCH severity classification, an SVM classifier-based MATLAB tool (R2015b) was used. There should be two severity levels, one from a 600 kPa impact (group 1) and one from a 650 kPa (group 2) impact. Data came from sampling at seven moments within 30 min in the Nos. 1–20 rabbits (mild group including Nos. 1–10, severe group including Nos. 11–20). At each sampling moment, 20 sets of MIPS data were collected. LOOCV was used for validation in each data set collected at one moment. One data sample was left out as a test sample, the remaining 19 were used as a training set. Each sample of the 20 was picked up in turn. Repeated classifications were performed on each of the 20 data sets that were acquired at one moment, and the accuracy of the MIPS data given in Table 1 is the average result of the 20 repetitions, which shows the classification accuracy of the MIPS data was above 90% for both CCH severity levels.

DISCUSSION

According to *Kim (2011)*, if TBI patients receive surgical treatment within 4 h of their injury, the mortality rate will decrease significantly. This means time is vital for most CCH

patients with a TBI. If patients' brain lesion information can be quickly obtained on the scene after an injury or on the way to the hospital, patients could get scheduled earlier for treatments, which could improve the prognosis of patients. The advantages of the MIPS technique include that it is noncontact, is highly sensitive in the early stage, can evaluate changes in hemorrhage for various locations, can be used as a real-time monitor prior to the hospital, and is expected to perform early clinical diagnoses of TBI-induced CCH.

In this work, CCH is formed by an impact on the selected parietal position of the head in rabbits. After being impacted, mechanical stress and shear forces can cause laceration of the parietal lobe. This can lead to a series of mechanical effects such as extrusion, tearing, and pulling near the brain impact or hedge position, due to the brain movement lagging behind the movement of the skull. Next, the brain tissue collides with the irregular inner surface of the skull to form inertial injuries, and it is also very likely that cavitation effects occur on the base of skull, causing artery rupture (*Xiong, Mahmood & Chopp, 2013*; *Margulies et al., 2015*; *Oehmichen et al., 2003*; *Dixon et al., 1994*; *Davis, 2000*). Hence, it is determined that CCH is caused by trauma, which is very different from an intracranial injection of blood that was reported by *Li et al. (2017b)* and *Pan et al. (2015)* in their process of forming injuries. The former is a spontaneous hemorrhage, the latter is a passive hemorrhage with a volume of three ml, which may be too large for the cranial cavity of a rabbit (*Sawyer, Everett & Green, 1954*). The animal model used in the experiment can cause CCH by adjusting the appropriate barometric pressure value on the impactor to control the volume of hemorrhage indirectly, which was verified as feasible in our CT experiment. We can conclude that this animal model has two advantages: one is optional injury location, and another is that it can avoid secondary injury compared to the weight drop model, due to the rabbit being fixed on the universal slab (*Xiong, Mahmood & Chopp, 2013*). The two advantages can make the injury more repeatable. However, the impactor lacks a sensor that can observe the instantaneous speed and acceleration at the impact location. These sensors are more direct indexes to describe the degree of injury in an animal (*Liu et al., 2016*; *Wu et al., 2016*) than the impact pressure, and we will add the sensor in future experiments.

Measurement of MIPS method is sensitive to movement of the target inside the coil *Jin et al. (2014a)*, so a marker was made on the experiment platform by a caliper for rough positioning, and two point sources that emit perpendicular light beam to the side and top of rabbit head for maintaining relatively consistent with coil sensor position when putting the rabbit back again after injury. Further, a verification experiment involved five healthy rabbits that measured the MIPS value of them when their heads inserted into the coil sensor twice. The result showed the difference of the mean MIPS value of the two positionings was approximately $0.37 \pm 0.92°$, which was much less than the minimal MIPS value of $-3.77 \pm 1.64°$ after injury described in the previous section, indicating the change of MIPS value in reentering to the coil sensor can be ignored compared with the MIPS value caused after injury, which did not affect the diagnosis of CCH rabbit in this study.

From the location of hemorrhage accumulation reflected by CT images, it is possible to come from a rupture of the pia mater, arachnoid and brain parenchyma after the impact.

A partial hemorrhage on the surface of the brain enters the lateral ventricle through the sagittal sinus, forming an early intracranial hemorrhage with flowing out of the vessel from the brain parenchyma. Since the mean brain conductivity reflected by the MIPS value is closely related to the volume proportion of the intracranial tissue and is positive correlation (*Griffiths, Stewart & Gough, 1999*), an alteration in the proportion of intracranial tissue volume caused by the continuous accumulation of intracranial hemorrhage can lead to change of conductivity indirectly, which is a pathological process involved in cerebrospinal fluid (CSF) compensation and cerebral blood flow (CBF) compensation (*Chen et al., 2017*). With the onset of compensation, changes in the proportion of intracranial tissue volume cause changes to the mean brain conductivity. The conductivity values of CSF, blood, gray matter, and white matter are 2.070, 1.210, 0.513, and 0.293 S/m at 65 MHz, respectively (*Gabriel, 1996*). During the compensation period with the volume of CSF and CBF decreasing, the mean brain conductivity declines and can lead to the MIPS value decreasing, which is consistent with the results of Fig. 9 that describe the MIPS values throughout the measurement period after injury and the result of Fig. 11 describes the MIPS values within 25 min after injury. When the CSF and CBF compensation are exhausted the hemorrhage accumulates continuously to cause a rise in the mean brain conductivity, resulting also in a rise of the MIPS value, which is consistent with the result of Fig. 11 that describes the last 5 min of measurement. Therefore, we can easily find that group 1 did not enter the compensation period, but group 2 entered the compensation period at 25 min, inferring that the CCH injury in group 2 was more severe than it was in group 1.

The proportion of intracranial tissue volume changes during cerebral autoregulation can be reflected by a MIPS curve. This demonstrates that the MIPS value is a functional diagnostic technique that can intervene before the appearance of structural brain lesions. Although ICP monitoring is the standard method of detection in the latest TBI guidelines (*Carney et al., 2017*), and *Li et al. (2017a)* and *Sun et al. (2016)* also proved that ICP monitoring has high sensitivity and accuracy in diagnosing brain lesions. Figure 13 from the study of *Wykes & Vindlacheruvu (2015)* revealed that ICP begins increasing after cerebral autoregulation is exhausted when the brain has entered a critical period. In addition, CT is not only a golden standard for diagnosing intracranial hemorrhage but also a necessary procedure in the trauma center after TBI (*Tonui et al., 2018*). Nevertheless, CT is limited to detect only structural lesions, but not functional lesions, because of its detection principle, which is based on the difference in the absorption of X-rays by objects so that it can describe abnormal structure anatomy and abnormal contrast enhancement (*Hernandez-Maraver et al., 2006*). *Sherer et al. (2009)* reported that the use of volumetric measurements of changes in tissue composition and cortical contusions makes it difficult to achieve the diagnostic accuracy needed for TBI, indicating that CT has some limitations in diagnosing brain functional lesions and may need to be combined with other diagnostic methods to improve its accuracy. As a result, the premise of TBI diagnosis based on CT and ICP monitoring depends on the appearance of structural lesions. However, the MIPS value has proven that it can make a diagnosis in the early stage, which would help to determine if there are functional
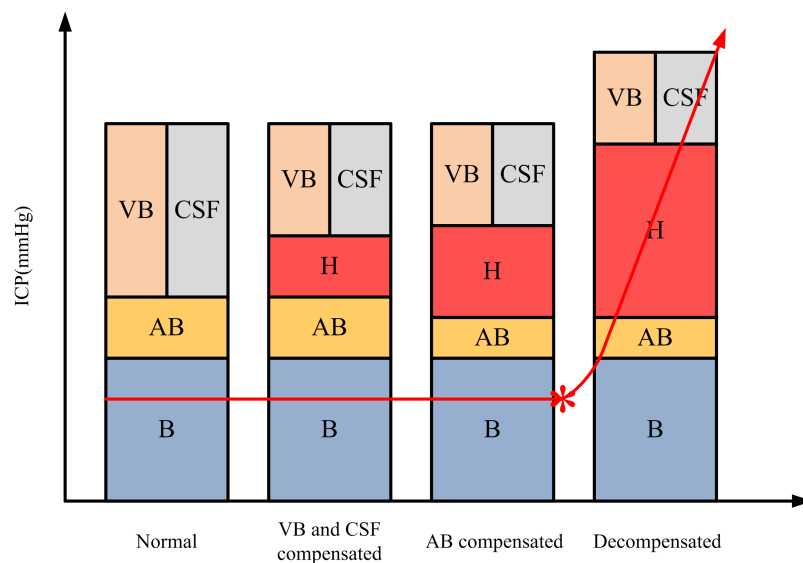
Figure 13 The main tissue content in the skull and ICP curve under normal, compensated, and decompensated conditions (*Wykes & Vindlacheruvu, 2015*). B, brain; AB, arterial blood; VB, venous blood; H, hemorrhage; CSF, cerebrospinal fluid.

lesions after TBI, indicating it is a potential, early diagnosis technique for most CCH in TBI.

There are several limitations in this work. First, it was not easy to achieve a quantitative measurement using a CT that serves people instead of animals because intracranial hemorrhages were diffuse in rabbits after their injuries. However, the severity of injury in group 1 and group 2 allowed the location, area and slices of the hemorrhage to be identified, so it can be used as a semiquantitative verification method, which has already achieved its purpose. Second, there is a series of complicated physiopathology pathways in the brain after TBI (*Prins et al., 2013*; *Kaur & Sharma, 2018*). During the acute stage after injury (≤ 1 h), a massive release of glutamate from presynaptic terminals disrupts ionic equilibrium on postsynaptic membranes, leading to an increase in released potassium (K^+) and calcium (Ca^{2+}) accumulation (*Ankarcrona et al., 1995*; *Mark et al., 2001*). Analogous processes like those aforementioncal ones may induce a change of the mean brain conductivity, which inturns affect the measurement results (*Aronowski & Zhao, 2011*; *Laufer, Solomon & Rubinsky, 2012*). Third, the number of samples is a defect for the stability of the classifier in this experiment, and we will expand the sample size in further work.

CONCLUSIONS

In this study, we made rabbits form two CCH severity levels through an impactor verified by CT, which was a way caused TBI closer to reality. A new diagnostic method for this TBI-induced CCH based on MIPS technology has the advantages of noncontact, portability and continuous monitoring. The MIPS results of CCH revealed that the MIPS value decreases gradually after injury if cerebral autoregulation was not exhausted or if it rises, which is consistent with changes in the mean brain conductivity. Also, linear

fitting of the MIPS value scatters more intuitively, which demonstrates the ability of MIPS method to distinguish CCH severity levels. These findings validate that the MIPS method is able to diagnose CCH after TBI, which is a potential technique for prehospital diagnosis. Further investigations include optimizing the coil sensor, which facilitates its capacity in multifrequency measurement.

ACKNOWLEDGEMENTS

The authors wish to thank Dr. Qingguang Yan support conducting this experiment.

Funding

This work were supported by the Foundation of the Third Military Medical University (2014XZH03) and the National Nature Science Foundation of China (61801483). The funders had no role in study design, data collection and analysis, decision to publish, or preparation of the manuscript.

Grant Disclosures

The following grant information was disclosed by the authors:
Third Military Medical University: 2014XZH03.
National Nature Science Foundation of China: 61801483.

Competing Interests

The authors declare that they have no competing interests.

Author Contributions

- Jun Yang conceived and designed the experiments, performed the experiments, analyzed the data, prepared figures and/or tables, authored or reviewed drafts of the paper, approved the final draft.
- Hui Zhao analyzed the data.
- Gen Li performed the experiments, analyzed the data, authored or reviewed drafts of the paper, approved the final draft.
- Qisheng Ran analyzed the data.
- Jingbo Chen performed the experiments, contributed reagents/materials/analysis tools, prepared figures and/or tables, authored or reviewed drafts of the paper.
- Zelin Bai performed the experiments, contributed reagents/materials/analysis tools, authored or reviewed drafts of the paper.
- Gui Jin he designed and implemented the algorithm of CCH severity classification.
- Jian Sun he designed and implemented the algorithm of CCH severity classification.
- Jia Xu contributed reagents/materials/analysis tools, authored or reviewed drafts of the paper.
- Mingxin Qin conceived and designed the experiments, approved the final draft.
- Mingsheng Chen conceived and designed the experiments, performed the experiments, prepared figures and/or tables, authored or reviewed drafts of the paper, approved the final draft.

Animal Ethics

The following information was supplied relating to ethical approvals (i.e., approving body and any reference numbers):

The protocol used was approved by the Laboratory Animal Welfare and Ethics Committee Of the Third Military Medical University (SYXK-20170002).

Data Availability

The raw data are available in the Supplemental Files.

Supplemental Information

Supplemental information for this article can be found online at http://dx.doi.org/10.7717/peerj.6717#supplemental-information.

REFERENCES

Amrhein TJ, Mostertz W, Matheus MG, Maass-Bolles G, Sharma K, Collins HR, Kranz PG. 2017. Reformatted images improve the detection rate of acute traumatic subdural hematomas on brain CT compared with axial images alone. *Emergency Radiology* 24(1):39–45 DOI 10.1007/s10140-016-1440-z.

Ankarcrona M, Dypbukt JM, Bonfoco E, Zhivotovsky B, Orrenius S, Lipton SA, Nicotera P. 1995. Glutamate-induced neuronal death: a succession of necrosis or apoptosis depending on mitochondrial function. *Neuron* 15(4):961–973 DOI 10.1016/0896-6273(95)90186-8.

Aronowski J, Zhao X. 2011. Molecular pathophysiology of cerebral hemorrhage. *Stroke* 42(6):1781–1786 DOI 10.1161/STROKEAHA.110.596718.

Carney N, Totten AM, O'Reilly C, Ullman JS, Hawryluk GW, Bell MJ, Bratton SL, Chesnut R, Harris OA, Kissoon N. 2017. Guidelines for the management of severe traumatic brain injury, Fourth Edition. *Neurosurgery* 80(1):6–15 DOI 10.1227/NEU.0000000000001432.

Cernak I. 2006. Recent advances in neuroprotection for treating traumatic brain injury. *Expert Opinion on Investigational Drugs* 15(11):1371–1381 DOI 10.1517/13543784.15.11.1371.

Chen S. 2003. Time course of cellular pathology after controlled cortical impact injury. *Experimental Neurology* 182(1):87–102 DOI 10.1016/S0014-4886(03)00002-5.

Chen M, Yan Q, Sun J, Jin G, Qin M. 2017. Investigating the relationship between cerebrospinal fluid and magnetic induction phase shift in rabbit intracerebral hematoma expansion monitoring by MRI. *Scientific Reports* 7(1):11186 DOI 10.1038/s41598-017-11107-1.

Davis AE. 2000. Mechanisms of traumatic brain injury: biomechanical, structural and cellular considerations. *Critical Care Nursing Quarterly* 23(3):1–13 DOI 10.1097/00002727-200011000-00002.

Di Ieva A, Schmitz EM, Cusimano MD. 2013. Analysis of intracranial pressure. *Neuroscientist* 19(6):592–603 DOI 10.1177/1073858412474845.

Dixon CE, Hamm RJ, Taft WC, Hayes RL. 1994. Increased anticholinergic sensitivity following closed skull impact and controlled cortical impact traumatic brain injury in the rat. *Journal of Neurotrauma* **11(3)**:275–287 DOI 10.1089/neu.1994.11.275.

Gabriel C. 1996. Tissue dielectric properties. *Available at* https://itis.swiss/virtual-population/tissue-properties/database/dielectric-properties/2018.

Giraudet F, Longeras F, Mulliez A, Thalamy A, Pereira B, Avan P, Sakka L. 2017. Noninvasive detection of alarming intracranial pressure changes by auditory monitoring in early management of brain injury: a prospective invasive versus noninvasive study. *Critical Care* **21(1)**:35 DOI 10.1186/s13054-017-1616-2.

Gonzalez CA, Rubinsky B. 2006. A theoretical study on magnetic induction frequency dependence of phase shift in oedema and haematoma. *Physiological Measurement* **27(9)**:829–838 DOI 10.1088/0967-3334/27/9/006.

Gonzalez CA, Valencia JA, Mora A, Gonzalez F. 2013. Volumetric electromagnetic phase-shift spectroscopy of brain edema and hematoma. *PLOS ONE* **8(5)**:e63223 DOI 10.1371/journal.pone.0063223.

Griffith J, Cluff K, Eckerman B, Aldrich J, Becker R, Moore-Jansen P, Patterson J. 2018. Non-invasive electromagnetic skin patch sensor to measure intracranial fluid–volume shifts. *Sensors* **18(4)**:1022 DOI 10.3390/s18041022.

Griffiths H, Stewart WR, Gough W. 1999. Magnetic induction tomography: a measuring system for biological tissues. *Annals of the New York Academy of Sciences* **873(1 ELECTRICAL BI)**:335–345 DOI 10.1111/j.1749-6632.1999.tb09481.x.

Hernandez-Maraver D, Hernandez-Navarro F, Gomez-Leon N, Coya J, Rodriguez-Vigil B, Madero R, Pinilla I, Martin-Curto LM. 2006. Positron emission tomography/computed tomography: diagnostic accuracy in lymphoma. *British Journal of Haematology* **135(3)**:293–302 DOI 10.1111/j.1365-2141.2006.06284.x.

Indraswari F, Wang H, Lei B, James ML, Kernagis D, Warner DS, Dawson HN, Laskowitz DT. 2012. Statins improve outcome in murine models of intracranial hemorrhage and traumatic brain injury: a translational approach. *Journal of Neurotrauma* **29(7)**:1388–1400 DOI 10.1089/neu.2011.2117.

Jin G, Sun J, Qin M, Chao W, Guo W, Yan Q, Peng B, Pan W. 2014a. A special phase detector for magnetic inductive measurement of cerebral hemorrhage. *PLOS ONE* **9(5)**:e97179 DOI 10.1371/journal.pone.0097179.

Jin G, Sun J, Qin M, Tang Q, Xu L, Ning X, Xu J, Pu X, Chen M. 2014b. A new method for detecting cerebral hemorrhage in rabbits by magnetic inductive phase shift. *Biosensors and Bioelectronics* **52**:374–378 DOI 10.1016/j.bios.2013.09.019.

Kaur P, Sharma S. 2018. Recent advances in pathophysiology of traumatic brain injury. *Current Neuropharmacology* **16(8)**:1224–1238 DOI 10.2174/1570159X15666170613083606.

Kellner CP, Sauvageau E, Snyder KV, Fargen KM, Arthur AS, Turner RD, Alexandrov AV. 2018. The VITAL study and overall pooled analysis with the VIPS non-invasive stroke detection device. *Journal of NeuroInterventional Surgery* **10(11)**:1079–1084 DOI 10.1136/neurintsurg-2017-013690.

Kim YJ. 2011. The impact of time from ED arrival to surgery on mortality and hospital length of stay in patients with traumatic brain injury. *Journal of Emergency Nursing* **37(4)**:328–333 DOI 10.1016/j.jen.2010.04.017.

Koessler L, Colnat-Coulbois S, Cecchin T, Hofmanis J, Dmochowski JP, Norcia AM, Maillard LG. 2017. In-vivo measurements of human brain tissue conductivity using focal

electrical current injection through intracerebral multicontact electrodes. *Human Brain Mapping* **38(2)**:974–986 DOI 10.1002/hbm.23431.

Laufer S, Solomon SB, Rubinsky B. 2012. Tissue characterization using electrical impedance spectroscopy data: a linear algebra approach. *Physiological Measurement* **33(6)**:997–1013 DOI 10.1088/0967-3334/33/6/997.

Li G, Ma K, Sun J, Jin G, Qin M, Feng H. 2017a. Twenty-four-hour real-time continuous monitoring of cerebral edema in rabbits based on a noninvasive and noncontact system of magnetic induction. *Sensors* **17(3)**:537 DOI 10.3390/s17030537.

Li G, Sun J, Ma K, Yan Q, Zheng X, Qin M, Jin G, Ning X, Zhuang W, Feng H, Huang S. 2017b. Construction of a Cerebral Hemorrhage Test System Operated in Real-time. *Scientific Reports* **7(1)**:42842 DOI 10.1038/srep42842.

Liljacyron A, Kelsen J, Andresen M, Fugleholm K, Juhler M. 2018. Feasibility of telemetric intracranial pressure monitoring in the neuro intensive care unit. *Journal of Neurotrauma* **35(14)**:1578–1586 DOI 10.1089/neu.2017.5589.

Liu W, Su S, Qiu J, Zhang Y, Yin Z. 2016. Exploration of pedestrian head injuries—collision parameter relationships through a combination of retrospective analysis and finite element method. *International Journal of Environmental Research and Public Health* **13(12)**:1250 DOI 10.3390/ijerph13121250.

Manwaring PK, Moodie KL, Hartov A, Manwaring KH, Halter RJ. 2013. Intracranial electrical impedance tomography. *Anesthesia & Analgesia* **117(4)**:866–875 DOI 10.1213/ANE.0b013e318290c7b7.

Margulies SS, Kilbaugh T, Sullivan S, Smith C, Propert K, Byro M, Saliga K, Costine BA, Duhaime A-C. 2015. Establishing a clinically relevant large animal model platform for TBI therapy development: using cyclosporin a as a case study. *Brain Pathology* **25(3)**:289–303 DOI 10.1111/bpa.12247.

Mark LP, Prost RW, Ulmer JL, Smith MM, Daniels DL, Strottmann JM, Brown WD, Hacein-Bey L. 2001. Pictorial review of glutamate excitotoxicity: fundamental concepts for neuroimaging. *American Journal of Neuroradiology* **22(10)**:1813–1824.

Mobashsher AT, Abbosh AM, Wang YF. 2014. Microwave system to detect traumatic brain injuries using compact unidirectional antenna and wideband transceiver with verification on realistic head phantom. *IEEE Transactions on Microwave Theory and Techniques* **62(9)**:1826–1836 DOI 10.1109/TMTT.2014.2342669.

Namjoshi DR, Good C, Cheng WH, Panenka W, Richards D, Cripton PA, Wellington CL. 2013. Towards clinical management of traumatic brain injury: a review of models and mechanisms from a biomechanical perspective. *Disease Models & Mechanisms* **6(6)**:1325–1338 DOI 10.1242/dmm.011320.

Nitsch JB, Rambousky R, Tkachenko S. 2015. Introduction of reflection and transmission coefficients for nonuniform radiating transmission lines. *IEEE Transactions on Electromagnetic Compatibility* **57(6)**:1705–1713 DOI 10.1109/TEMC.2015.2456098.

Oehmichen M, Walter T, Meissner C, Friedrich HJ. 2003. Time course of cortical hemorrhages after closed traumatic brain injury: statistical analysis of posttraumatic histomorphological alterations. *Journal of Neurotrauma* **20(1)**:87–103 DOI 10.1089/08977150360517218.

Oziel M, Korenstein R, Rubinsky B. 2017. Radar based technology for non-contact monitoring of accumulation of blood in the head: a numerical study. *PLOS ONE* **12(10)**:e0186381 DOI 10.1371/journal.pone.0186381.

Pan W, Yan Q, Qin M, Jin G, Sun J, Ning X, Zhuang W, Peng B, Li G. 2015. Detection of cerebral hemorrhage in rabbits by time-difference magnetic inductive phase shift spectroscopy. *PLOS ONE* **10(5)**:e128127 DOI 10.1371/journal.pone.0128127.

Pandey S, Sharma V, Singh K, Pandey D, Sharma M, Patil DB, Shende N, Chauhan RS. 2017. Bilateral traumatic intracranial hematomas and its outcome: a retrospective study. *Indian Journal of Surgery* **79(1)**:19–23 DOI 10.1007/s12262-015-1416-3.

Prins M, Greco T, Alexander D, Giza CC. 2013. The pathophysiology of traumatic brain injury at a glance. *Disease Models & Mechanisms* **6(6)**:1307–1315 DOI 10.1242/dmm.011585.

Pugh MJ, Finley EP, Wang CP, Copeland LA, Jaramillo CA, Swan AA, Elnitsky CA, Leykum LK, Mortensen EM, Eapen BA, Noel PH, Pugh JA, The TRACC Research Team. 2016. A retrospective cohort study of comorbidity trajectories associated with traumatic brain injury in veterans of the Iraq and Afghanistan wars. *Brain Injury* **30(12)**:1481–1490 DOI 10.1080/02699052.2016.1219055.

Robertson CS, Zager EL, Narayan RK, Handly N, Sharma A, Hanley DF, Garza H, Maloney-Wilensky E, Plaum JM, Koenig CH, Johnson A, Morgan T. 2010. Clinical evaluation of a portable near-infrared device for detection of traumatic intracranial hematomas. *Journal of Neurotrauma* **27(9)**:1597–1604 DOI 10.1089/neu.2010.1340.

Sawyer CH, Everett JW, Green JD. 1954. The rabbit diencephalon in stereotaxic coordinates. *Journal of Comparative Neurology* **101(3)**:801–824 DOI 10.1002/cne.901010307.

Schwindling L, Ragoschke-Schumm A, Kettner M, Helwig S, Manitz M, Roumia S, Lesmeister M, Grunwald IQ, Fassbender K. 2016. Prehospital imaging-based triage of head trauma with a mobile stroke unit: first evidence and literature review. *Journal of Neuroimaging* **26(5)**:489–493 DOI 10.1111/jon.12355.

Sherer M, Stouter J, Hart T, Nakase-Richardson R, Olivier J, Manning E, Yablon SA. 2009. Computed tomography findings and early cognitive outcome after traumatic brain injury. *Brain Injury* **20(10)**:997–1005 DOI 10.1080/02699050600677055.

Song J, Chen R, Yang L, Zhang G, Li W, Zhao Z, Xu C, Dong X, Fu F. 2018. Electrical impedance changes at different phases of cerebral edema in rats with ischemic brain injury. *BioMed Research International* **2018(11)**:1–10 DOI 10.1155/2018/9765174.

Sun J, Jin G, Li G, Chen Y, Qin M. 2016. The experimental study of increased ICP on cerebral hemorrhage rabbits with magnetic induction phase shift method. *Iranian Journal of Medical Physics* **13(2)**:125–136 DOI 10.22038/IJMP.2016.7458.

Sun J, Jin G, Qin MX, Wan ZB, Wang JB, Wang C, Guo WY, Xu L, Ning X, Xu J, Pu XJ, Chen MS, Zhao HM. 2014. Detection of acute cerebral hemorrhage in rabbits by magnetic induction. *Brazilian Journal of Medical and Biological Research* **47(2)**:144–150 DOI 10.1590/1414-431X20132978.

Tonui PM, Spilman SK, Pelaez CA, Mankins MR, Sidwell RA. 2018. Head CT before transfer does not decrease time to craniotomy for TBI patients. *American Surgeon* **84(2)**:201–207.

Wang H, Gao J, Lassiter TF, Mcdonagh DL, Sheng H, Warner DS, Lynch JR, Laskowitz DT. 2006. Levetiracetam is neuroprotective in murine models of closed head injury and subarachnoid hemorrhage. *Neurocritical Care* **5(1)**:71–78 DOI 10.1385/ncc:5:1:71.

Wu LC, Nangia V, Bui K, Hammoor B, Kurt M, Hernandez F, Kuo C, Camarillo DB. 2016. In Vivo evaluation of wearable head impact sensors. *Annals of Biomedical Engineering* **44(4)**:1234–1245 DOI 10.1007/s10439-015-1423-3.

Wykes V, Vindlacheruvu R. 2015. Intracranial pressure, cerebral blood flow and brain oedema. *Surgery (Oxford)* **33(8)**:355–362 DOI 10.1016/j.mpsur.2015.06.001.

Xiong Y, Mahmood A, Chopp M. 2013. Animal models of traumatic brain injury. *Nature Reviews Neuroscience* **14(2)**:128–142 DOI 10.1038/nrn3407.

Zeiler FA, Thelin EP, Helmy A, Czosnyka M, Hutchinson PJA, Menon DK. 2017. A systematic review of cerebral microdialysis and outcomes in TBI: relationships to patient functional outcome, neurophysiologic measures, and tissue outcome. *Acta Neurochirurgica* **159(12)**:2245–2273 DOI 10.1007/s00701-017-3338-2.